Biometals (2011) 24:357–375
DOI 10.1007/s10534-010-9405-2

Heterogenous distribution of ferroportin-containing neurons in mouse brain

Michael W. Boserup · Jacek Lichota · David Haile · Torben Moos

Received: 13 March 2010 / Accepted: 22 December 2010 / Published online: 7 January 2011

Abstract Iron is crucial for a variety of cellular functions in neuronal cells. Neuronal iron uptake is reflected in a robust and consistent expression of transferrin receptors and divalent metal transporter 1 (DMT 1). Conversely, the mechanisms by which neurons neutralize and possibly excrete iron are less clear. Studies indicate that neurons express ferroportin which could reflect a mechanism for iron export. We mapped the distribution of ferroportin in the adult mouse brain using an antibody prepared from a peptide representing amino acid sequences 223–303 of mouse ferroportin. The antibody specifically detected ferroportin in brain homogenates, whereas homogenates of cultured endothelial cells were devoid of immunoreactivity. In brain sections, ferroportin was confined to neuronal cell bodies and peripheral processes of cerebral cortex, hippocampus, thalamus, brain stem, and cerebellum. In brain stem ferroportin-labeling was particularly high in neurons of cranial nerve nuclei and reticular formation. Ferroportin was hardly detectable in striatum, pallidum, or hypothalamus. Among non-neuronal cells, ferroportin was detected in oligodendrocytes and choroid plexus epithelial cells. A comparison with previous studies on the distribution of transferrin receptors in neurons shows that many neuronal pools coincide with those expressing ferroportin. The data therefore indicate that neuronal iron homeostasis consists of a delicate balance between transferrin receptor-mediated uptake of iron-transferrin and ferroportin-related iron excretion. The findings also suggest a particular high turnover of iron in neuronal regions, such as habenula, hippocampus, reticular formation and cerebellum, as several neurons in these regions exhibit a prominent co-expression of transferrin receptors and ferroportin.

Keywords Blood–brain barrier · Iron · Neurodegeneration · Oxidative stress · qPCR · Transferrin

Abbreviations

3N	Oculomotor nucleus
3V	3rd ventricle
5N	Motor trigeminal nucleus
7N	Facial nucleus
M1	Primary motor cortex
Amb	Ambiguus nucleus
bEnd3	Mouse brain endothelial cells
CA1	Field CA1 of Ammon's horn
CA2	Field CA2 of Ammon's horn
CA3	Field CA3 of Ammon's horn
cc	Corpus callosum

M. W. Boserup · J. Lichota · T. Moos (✉)
Section of Neurobiology, Biomedicine, Department of Health Science and Technology, Aalborg University, Fr. Bajers Vej 3B, 1.216, 9220 Aalborg East, Denmark
e-mail: tmoos@hst.aau.dk

D. Haile
South Texas Veterans Health Care System, San Antonio, TX, USA

CP	Choroid plexus
D3V	Dorsal part of the third ventricle
DAB	3,3-Diaminobenzidine tetrahydrochloride
DG	Dentate gyrus
DMT 1	Divalent metal transporter 1
DR	Dorsal raphe nucleus
EPl	External plexiform layer of the olfactory bulb
EPlA	External plexiform layer of the accessory olfactory bulb
Fpn-ir	Ferroportin-immunoreactivity
Gl	Glomerular layer of the olfactory bulb
GrO	Granular cell layer of the olfactory bulb
hbc	Habenular commissure
hi	Habenulo-interpeduncular tract
IntP	Interposed cerebellar nucleus posterior part
IG	Induseum griseum
IP	Interpeduncular nucleus
IPl	Internal plexiform layer of the olfactory bulb
Lat	Lateral cerebellar nucleus
LC	Locus coeruleus
LHb	Lateral habenular nucleus
ME	Median eminence
Med	Medial cerebellar nucleus
MHb	Medial habenular nucleus
Mi	Mitral cell layer of the olfactory bulb
Pir	Piriform cortex
PPBS	Potassium phosphate-buffered saline
Rbd	Rhabdoid nucleus
RT	Reverse transcriptase
TSA	Tyramid signal amplification
UTR	Untranslated region
VM	Ventral medial thalamic nucleus

Introduction

Iron plays a vital role in many important functions throughout the body, including the brain. Acting as co-factor for important enzymes, iron is an essential determinant for the synthesis of neurotransmitters in neurons, and for the synthesis of myelin-proteins and fatty acids in oligodendrocytes, thereby requiring a continuous need for the brain to absorb iron from the circulation (Crichton 2009; Rouault and Cooperman 2006; Todorich et al. 2009; Zecca et al. 2004). The demand for a continuous iron transport into the brain presents a permanent challenge, even superseded by the fact that excess iron is not tolerated very well by the brain. Its accumulation has been associated with an iron-catalyzed production of free radicals that leads to neuronal damage (Altamura and Muckenthaler 2009; Crichton 2009; Jeong et al. 2009; Rouault and Cooperman 2006; Zecca et al. 2004; Zhu et al. 2007). Consequently, the brain needs to keep its iron level within a steady range by balancing uptake and export.

At the organ level, iron uptake by the brain takes place at the blood–brain barrier and blood–cerebrospinal fluid barriers via specific internalization of iron-transferrin and transferrin receptors (Moos et al. 2007). The export of iron from the brain occurs non-specifically via absorption of cerebrospinal fluid at the arachnoid villi at the interface between the dura mater and the arachnoid membrane (Balin et al. 1986; Moos and Morgan 1998). At the cellular level, the handling of iron in the brain is more complex due to the fact that some cell types, particularly the neurons, seem capable of regulating their iron levels through uptake, storage and excretion. Hence, neurons simultaneously express transferrin receptors for uptake, ferritin for storage, and also seem capable of exporting iron via expression of the ferrous iron-exporter ferroportin (cf. Moos et al. 2007).

The ferroportin molecule (also known as metal transporter protein 1 or Ireg-1 and Metal Transporter Protein 1 or MTP1; gene symbol Slc40a1) is a transmembrane protein considered to be the only one capable of exporting iron from cells (Abboud and Haile 2000; Donovan et al. 2000; McKie et al. 2000). It was initially detected in duodenal enterocytes, placental trophoblasts, and macrophages of the liver and spleen (Abboud and Haile 2000; Donovan et al. 2000; McKie et al. 2000). Its significance for iron export across cellular membranes was revealed in studies of the mutated ferroportin gene in mice which showed that loss of ferroportin function leads to severe cellular iron accumulation (Donovan et al. 2005; Zohn et al. 2007), the main reason being elevated iron absorption in duodenal enterocytes due to a lack of hepcidin which regulates the expression of ferroportin (Nemeth et al. 2004). The elevated iron transport into the body leads to a profoundly elevated level of iron in the circulation. This in turn causes diffuse iron storage in the body, thereby mimicking the clinical features of hemochromatosis in man (Chua et al. 2007).

Ferroportin was detected in discrete brain regions of the mouse (Wu et al. 2004), rat (Burdo et al. 2001; Moos and Rosengren Nielsen 2006), and man (Koeppen et al. 2007). These studies revealed a prominent neuronal expression of ferroportin in regions like the cerebral cortex, hippocampus, and cerebellum, whereas the opposite seemed to apply to regions like the striatum and thalamus (Burdo et al. 2001; Koeppen et al. 2007; Moos and Rosengren Nielsen 2006; Wu et al. 2004). Despite the fact that these studies have provided evidence of ferroportin expression, a detailed mapping of its spatial distribution pattern would nonetheless enhance the understanding of ferroportin as an iron exporter throughout the brain. In this study, we set out to perform a complete mapping of ferroportin in the adult mouse brain using an antibody generated against mouse ferroportin (Abboud and Haile 2000). We also verify the expression of ferroportin in the brain by means of gene and protein detection in micro-dissected samples.

Experimental procedures

Animals

Sixteen 8-week-old male mice of the 129/SvJ strain (Taconic, Ry, DK) were used for the study. The animals had free access to water and food and were housed in cages at the Animal Department of Aalborg Hospital, Aalborg under constant temperature and humidity conditions, and kept on a 12 h light/dark cycle. The procedures dealing with the handling of animals described in this study were approved by the Danish Experimental Animal Inspectorate under the Ministry of Justice.

Tissue preparation

For immunohistochemical studies, mice ($n = 6$) were deeply anesthetized with 3 ml Avertin/100 g animal (1.87 g tribromoethanol (Sigma-Aldrich, Copenhagen, DK) dissolved in 2 ml 99% ethanol added to 98 ml distilled H_2O and heated until completely dissolved). The animals were then perfused transcardially via the left ventricle, first with heparin (15,000 IE/l) in 0.1 M potassium phosphate-buffered saline (PPBS) for half a minute, and then with 4% w/v paraformaldehyde in 0.1 M PPBS, pH 7.4. The brains were gently dissected, post-fixed for 4 h at room temperature and immersed in 30% sucrose-PPBS for 48 h. Subsequently, the brains were cut into serial, coronal 40 μm sections on a cryostat and stored in PPBS at 4°C until later immunohistochemical processing of the free-floating sections.

For biochemical analyses, the brains of deeply anesthetized animals were dissected on ice under a dissecting microscope to isolate either the whole brain ($n = 5$) or the habenular region ($n = 5$). The latter is situated in the region of the dorsal thalamus that extends from −0.82 to – 2.18 mm from bregma (Franklin and Paxinos 2008) and was used for PCR analyses (see below) and western blotting experiments. For the latter, the dissected brain tissue was rapidly homogenized in Laemmli buffer with 2% SDS and 2 mM mercaptoethanol in an Ultra Turrax T25 homogenizer. The total homogenate was examined by gel electrophoresis, and the intensity of the bands on the Coomassie blue stained SDS PAGE determined the amount of sample to be added to wells for the Western blotting. Immortalised mouse brain endothelial cells (bEnd3) were processed in the same manner. The bEnd3 were cultured in media for 6 days until they reached confluence (Gosk et al. 2008), and then homogenized using the protocol described above. Dissected habenular tissue was also used for PCR analyses (see below).

Immunohistochemistry

The sections were subjected to single-labeling immunohistochemistry to map the distribution of ferroportin, and all steps in the procedure were carried out under gentle agitation. The sections were preincubated in 1.5% normal swine serum diluted in 0.1 M PPBS, pH 7.4 with 0.15% Triton X-100 (Sigma, Copenhagen, DK), for 15 min at room temperature to block any unspecific binding. They were then incubated overnight at 4°C with an antibody prepared from a peptide representing amino acid sequences 223–303 of mouse ferroportin (Abboud and Haile 2000) diluted 1:1000 in blocking buffer. This antibody has been shown to detect ferroportin specifically in various organs of the body, including the brain [Abboud and Haile 2000 (fetal mouse);

Burdo et al. 2001 (adult rat); Koeppen et al. 2007 (man); Moos and Rosengren Nielsen 2006 (developing rat)]. The following day, the antibody was visualized with the ABC-system; in brief, the sections were incubated for 30 min at room temperature in biotinylated swine anti-rabbit (DAKO, Glostrup, DK) diluted 1:300. They were then incubated for 15 min in the ABC–streptavidin–peroxidase complex (Vectastain Elite ABC kit, Vector laboratories, Rodovre, DK) prepared according to the manufacturer's recommendation (one drop of reagent A plus one drop of reagent B in 10 ml TBS/Nonidet). The sections were then subjected to tyramide signal amplification (TSA) (PerkinElmer, Skovlunde, DK) diluted 1:100 for 5 min, and incubated again in the ABC–streptavidin–peroxidase complex for 15 min. The sections were finally reacted for 10 min in 0.015% H_2O_2 in 0.05% 3,3-diaminobenzidine tetrahydrochloride (DAB), pH 7.0. Throughout most of the procedure, the sections were washed in PPBS with blocking buffer 1:40 for 3 × 5 min between each step. However, prior to the TSA and DAB incubation steps, the sections were rinsed 3 × 5 min in Tris–HCl buffer pH 7.0 to avoid phosphate ions in the reaction buffer. The free-floating sections were mounted on lysine-coated glass slides, dried, and embedded in Pertex Mounting Media (Cellpath Plc, Newtown, UK). In order to make sure that the secondary antibody did not bind non-specifically to any structures, control sections were incubated as described above, but without the primary antibody. Immunolabeling was not observed in any of the control sections, indicating that the detection system did not reveal unwanted non-specific labeling.

Additional sections were processed for immunofluorescence histochemistry (Moos et al. 2006). Ferroportin was co-detected with transferrin receptors that are expressed by neurons and brain capillary endothelial cells in the mouse brain (Moos 1996). The anti-ferroportin antibody was diluted 1:1000 in blocking buffer together with rat anti-transferrin receptor antibody (AbDSerotec, Düsseldorf, Germany) diluted 1:100 overnight at 4°C. The next day, the antibodies were detected with biotinylated swine anti-rabbit (DAKO, Glostrup, DK) diluted 1:300 followed by streptavidin-Alexa 488 (Invitrogen, Taastrup, DK) diluted 1:200 and Qdot 605-conjugated goat anti-rat IgG (Invitrogen, Taastrup, DK) diluted 1:200.

Data collection and analyses

A standard atlas of the mouse brain was used for identification of the labeled neuroanatomical areas (Franklin and Paxinos 2008). Ferroportin-immunoreactive cells in the mouse brain were estimated semi-quantitatively using a five-degree score based on the immunoreactivity in cell bodies and peripheral processes (Table 1). The sections were examined and documented photographically with an Axioplan 2 Imaging Microscope (Zeiss, Ger), equipped with Nomarski Interference Contrast (Nomarski optics), and fitted with an AxioCam MRc digital camera (Zeiss, Ger). Nomarski optics is a technique suitable to enhance the contrast imaging in lightly stained or unstained sections. The captured images were adjusted for contrast and brightness using Adobe Photoshop CS2 software.

PCR-analyses

Total RNA was extracted from brain tissue containing the habenula with the NucleoSpin® RNA II kit (Macherey-Nagel, Düren, Ger) and cDNA synthesis conducted with 1 μg RNA in 20 μl reagent from the iScript™ cDNA synthesis kit (Bio-Rad, Copenhagen, DK). Reverse transcriptase (RT)-PCR carried out with 1 μl cDNA using the following primers: Ferroportin forward, CCCTGCTCTGGCTGTAAAAG, Ferroportin reverse, AACAAGGCCACATTTTCG AC and DreamTaq™ Green PCR Master Mix (Fermentas, Helsingborg, Sw). A Veriti 96 Well Thermal cycler (Applied Biosystems, Naerum, DK) was used for the following program: 1×: 95°C 1 min; 30×: 95°C 15 s; 55°C 15 s; 72°C 15 s; 1×: 72°C 7 min. The control reaction (RT-) was performed identically except for the fact that 1 μl total RNA was used instead of cDNA as a template.

qRT-PCR analyses of brain samples containing the habenula, duodenum and cultured bEnd3 cells were performed using the Stratagene Mx 3000 system. The ferroportin primers were the same as used for RT-PCR. As a control for normalization, the following Gapdh primers were used: forward 5′ AACGACCC CTTCATTGAC 3′, reverse 5′ TCCACGACATACT CAGCAC 3′. The duodenal Fpn/Gapdh ratio was considered 100%, and the Fpn/Gapdh signals of brain and bEnd3 cells were expressed relatively to that of the duodenum.

Table 1 Distribution of ferroportin-like immunoreactivity in adult mouse CNS

	Cell bodies	Peripheral processes
Neuronal expression		
Cerebral cortex		
Frontal, motor, piriform, retrospinal, sensory	−	+++
Parietal, occipital, temporal	−	++
Agranular insular, cingulate, entorhinal, perirhinal	−	+
Orbital	−	−
Basal ganglia and basal forebrain		
Accumbens ncl.	+	−
Basal ncl. (Meynert)	+	−
Globus pallidus	+	−
Caudate-putamen, entopeduncular ncl, ventral pallidum	−	−
Limbic structures		
Amygdaloid nuclear complex	+	−
Lateral septal ncl.	+	−
Medial septal ncl.	+	−
CA1, CA2, CA3	−	++++
Dentate gyrus	−	++++
Indusium griseum	−	++++
Olfactory system		
External plexiform layer of the olfactory bulb	−	++++
External plexiform layer of the accessory olfactory bulb	−	++++
Mitral layer of the accessory olfactory bulb	−	+++
Internal plexiform layer of the olfactory bulb	−	++
Mitral layer of the olfactory bulb	−	++
Lateral olfactory tract	−	+
Dorsal lateral olfactory tract	−	+
Glomerular layer	−	+
Granule cell layer of the olfactory bulb	−	−
Thalamus		
Medial habenular ncl.	++	++++
Ventral medial thalamic ncl.	++	++
Ventral posterolateral thalamic ncl.	++	−
Ventral posteromedial thalamic ncl.	++	−
Lateral posterior thalamic ncl.	++	−
Lateral habenular ncl.	+	−
Posterior thalamic nuclear group	+	−
Reticular thalamic nucleus	+	−
Subthalamic ncl.	−	−
Hypothalamus		
Dorsomedian ncl.	+	−
Paraventricular ncl., supraoptic ncl.	+	−
Median eminence	−	+++
Mesencephalon		
Oculomotor ncl.	+++	+
Trochlear ncl.	+++	+

Table 1 continued

	Cell bodies	Peripheral processes
Red ncl.	++	−
Substantia nigra pars compacta	++	−
Superior colliculus	++	.
Substantia nigra pars reticulata	+	−
Mesencephalic trigeminal ncl.	+	−
Ventral tegmental area	+	−
Interpeduncular ncl.	−	++++
Pons		
Motor trigeminal ncl., facial ncl.	+++	++
Abducens ncl.	+++	+
Locus coeruleus	+++	−
Pontine ncl.	++	−
Dorsal and ventral cochlear nuclei	++	−
Vestibular nuclei	++	−
Medulla oblongata		
Ambiguus ncl.	+++	+
Ncl of the solitary tract, medial part	+++	+
Hypoglossal ncl.	++	−
Dorsal motor ncl. of the vagus	+	−
Reticular formation		
Pontine reticular nucleus	+++	+++
Ventral and laterodorsal tegmental nuclei	+++	+
Dorsal raphe ncl., rhabdoid nucleus	+	++++
Medial longitudinal fasciculus	−	++
Cerebellum		
Purkinje cells	+++	++++
Medial, interposed, and lateral (dentate) nuclei	++	−
Non-neuronal expression		
Oligodendrocytes	++	−
Astrocytes	−	−
Microglia	−	−
Choroid plexus epithelium	++	−
Endothelial cells	−	−
Ependymal cells	−	−

Symbols are related to the density of individual cells bodies or their peripheral processes (axons/dendrites) exhibiting ferroportin-like immunoreactivity, which was semi-quantitatively assessed in five degrees: Very strong ++++, strong +++, moderate ++, weak +, not detectable −

ncl. nucleus, *n.d.* not determined

Western blotting

Brain homogenates of the habenular region were blotted together with bEnd3 cells. The samples were dissolved in NuPAGE LDS buffer (Invitrogen, Taastrup, DK) with 0.25% mercaptoethanol (Sigma, Copenhagen, DK) and heated for 10 min at 70°C before being added to NuPAGE (4–12% Bis–Tris Gel with MOPS running buffer (Invitrogen, Taastrup, DK) with 0.25% mercaptoethanol) and transferred to 0.20 μm nitrocellulose membranes (LKB, Sw) in NuPAGE transfer buffer (Invitrogen, Taastrup, DK)

mixed with 10% methanol to ensure optimal protein transfer. The membranes were blocked for non-specific binding of the antibodies by incubating them for 60 min with 2% Tween-20 and 3% skim milk powder dissolved in 0.1 M PBS, pH 7.4. The nitrocellulose membranes were then incubated overnight at 4°C with mouse-anti ferroportin diluted 1:2000 in 0.1 M PBS, pH 7.4 containing 0.05% Tween-20. Antibody-binding was detected with peroxidase-coupled swine anti-rabbit immunoglobulin (GE Healthcare, Hillerod, DK) diluted 1:3000 for 30 min at room temperature, and visualized with ECL (GE Healthcare, Hillerod, DK) in a Kodak Photoreader Image Station 4000 MM Pro.

Results

Biochemical analyses

The RT-PCR-analysis revealed the presence of a Fpn transcript that did not appear in the control samples processed without reverse transcriptase (not shown). The qPCR analysis from the brain and bEnd3 cells samples clearly showed a lower expression of Fpn compared to the duodenum. The expression by the brain containing the habenular region was approximately 7.5% and the bEnd3 only 0.5% (Fig. 1). The amount of Fpn transcript in the bEnd3 cells was consistently low, but significantly higher when compared to no template control (not shown). Western blots were carried out on samples obtained from homogenates of whole brains, the habenular region, and bEnd3. The brain homogenates and the habenular samples consistently produced a band of ferroportin with a molecular weight of 75–80 kDa, whereas the bEnd3 samples were negative (Fig. 2).

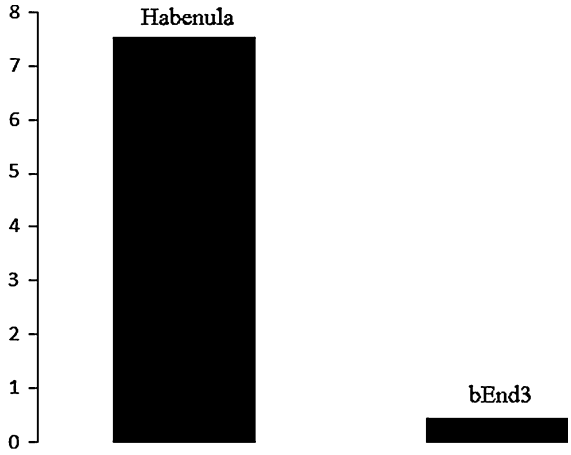

Fig. 1 qPCR analysis of ferroportin expression in micro-dissected preparations of the mouse habenular and cultured bEnd3 cells. The expression of ferroportin mRNA, normalized with Gapdh, in habenula and bEnd3 cells was correlated to the expression in the duodenum, which arbitrarily was set to 100%

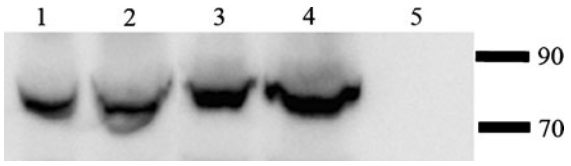

Fig. 2 Western blots with a ferroportin protein band corresponding to a molecular weight of 75–80 kDa in preparations of total brain (*lane 1–2*) and micro-dissected preparations of the habenula (*lane 3–4*). Ferroportin is not detected in homogenates of immortalized mouse brain capillary endothelial cells (bEnd3) (*lane 5*)

Cellular localization of ferroportin immunoreactivity

Ferroportin-immunoreactivity (Fpn-ir) was observed in neurons throughout the brain and was confined to cell bodies and neuronal processes. The immunolabeled neuronal processes could be identified as axons and proximal dendrites by the obvious Fpn-ir in representative processes of both, e.g., in axons of the neurons that project from the medial habenular nucleus to the interpeduncular nucleus and in proximal dendrites of neurons of Purkinje cells (see below). The presence of Fpn-ir in axons, however, was not a consistent phenomenon as some white matter tracts like the corpus callosum and pyramidal tract were devoid of Fpn-ir labeled elements (not shown).

Among non-neuronal cells, Fpn-ir was observed in oligodendrocytes in which the cell body-cytoplasm was labeled without labeling of peripheral processes (Fig. 3a). Neither astrocytes nor microglia were labeled. Fpn-ir was seen in choroid plexus epithelial cells of the ventricles (Fig. 3b). In contrast, Fpn-ir was not seen detected in brain capillary endothelial cells (Fig. 3c, d). The endothelial cells were not labeled with Fpn-ir in vivo in simple brain capillaries or within endothelial cells of arteries like those of the basal artery or within endothelial cells of veins like

those of the superior sagittal suture. The lack of Fpn-ir in brain capillary endothelial cells also applied to the endothelial cells of the capillaries of circumventricular organs (not shown). Double-labeling immunofluorescence histochemistry revealed that transferrin receptor-immunoreactivity was present in neurons and brain capillaries (Fig. 3e, e′), whereas Fpn-ir was confined to neurons (Fig. 3d–f′). Fpn-ir was not seen in ependymal cells (Fig. 3g).

The regional distribution of neuronal ferroportin

Neuronal Fpn-ir elements were distributed throughout the various nuclei and regions of the cerebral cortex, basal ganglia and basal forebrain, limbic structures, olfactory system, diencephalon, mesencephalon, pons, medulla oblongata, reticular formation, and cerebellum. The distribution of ferroportin in various regions of the mouse brain is summarized in Table 1.

Cerebral cortex

Fpn-ir intensity varied in the neurons throughout the cerebral cortex (Fig. 4). Neuronal Fpn-ir was detected in peripheral processes, but not in their corresponding cell bodies (Fig. 4a). The Fpn-ir was most prominent in the frontal (Fig. 4a), motor, sensory, retrosplenial, and piriform cortices (Fig. 4b). Moderate Fpn-ir was seen in the occipital, parietal, and temporal areas, whereas weak Fpn-ir was found in the agranular insular, cingulate, entorhinal, and perirhinal areas. Neuronal Fpn-ir was not seen in the orbital cortex.

Basal ganglia and basal forebrain

Many components of the basal ganglia—the caudate-putamen (striatum), entopeduncular nucleus, and ventral pallidum—were devoid of neuronal Fpn-ir in both cell bodies and their peripheral processes. A weak Fpn-ir was detected in neuronal cell bodies in the globus pallidus. Neurons of the compact part of the substantia nigra that project to the caudate-putamen did exhibit Fpn-ir in their cell bodies (see below). Weak Fpn-ir was seen in the soma of neurons of the basal nucleus (Meynert) and nucleus accumbens (not shown).

Fig. 3 The cellular distribution of ferroportin-immunoreactivity (Fpn-ir) in the mouse brain. **a** Section of the habenular commisure (hbc) overlying the dorsal part of the third ventricle (D3V) showing Fpn-ir in interfascicular oligodendrocytes (*arrows*). *Insert* Fpn-ir in a single oligodendrocyte shown at high-power magnification. The immunolabeling is confined to the cell cytoplasm. **b** Section of the lateral ventricle showing Fpn-ir in the choroid plexus (CP) marked with an *arrow*. **c**, **d** Absence of Fpn-ir in brain capillaries. **c** Section from the cerebral cortex. Fpn-ir is present in neurons (*arrow*), but absent from a brain capillary (*asterisk*). **d** High contrast image of section from the corpus callosum showing unlabeled brain capillaries (*asterisks*). **e**, **f** Double-immunofluorescence detecting transferrin receptors (**e**) and ferroportin (**f**) within the same section of the brain stem. **e** Transferrin receptors are present in brain capillaries (*thin arrows*) and neurons. **f** In contrast, ferroportin is only detected in neurons. **e′**, **f′** Part of the section shown in **e** and **f** showing a brain capillary at high magnification. Only transferrin receptors are detected (**e′**), whereas the capillary is devoid of ferroportin immunoreactivity (**f′**). **g** Section from the wall of the third ventricle shown at high-power magnification. Fpn-ir is absent from ependymal cells marked with an *asterisk* (Nomarski optics). *Scale bars* **a**, **b** = 80 μm; **c**, **d**, **g** = 10 μm; **e**, **f** = 40 μm; **a** *insert* = 5 μm; **e′**, **f′** = 20 μm

Limbic structures

In the hippocampus, neuronal Fpn-ir was prominent in the cortical field areas of CA1, CA2 and CA3 of Ammon's horn (Fig. 5a–c). This labeling was confined to peripheral processes, most likely axons of the neurons originating from the hippocampal cortex (Fig. 5b, c). A labeling of similar intensity was seen in neuronal processes of the dentate gyrus (Fig. 5d). It was practically impossible to detect Fpn-ir within neuronal cell bodies in the hippocampus. The indusium griseum that receives afferent projections from the hippocampal region CA1, and may be considered an integrated part of the hippocampus (Adamek et al. 1984), exhibited a robust labeling of neuronal processes clearly suggesting that ferroportin is present in axons of the pyramidal neurons of the hippocampus (Fig. 5e–g). In the septal area, neurons of the lateral and medial septal nuclei contained Fpn-ir; the labeling being confined to neuronal cell bodies without labeling of peripheral processes. This observation also applied to neurons of the amygdaloid nuclear complex. The Fpn-ir was equally distributed within neurons of the different amygdaloid nuclei.

Olfactory system

Neuronal fibers of the external plexiform layer of the olfactory bulb and the external plexiform layer of the

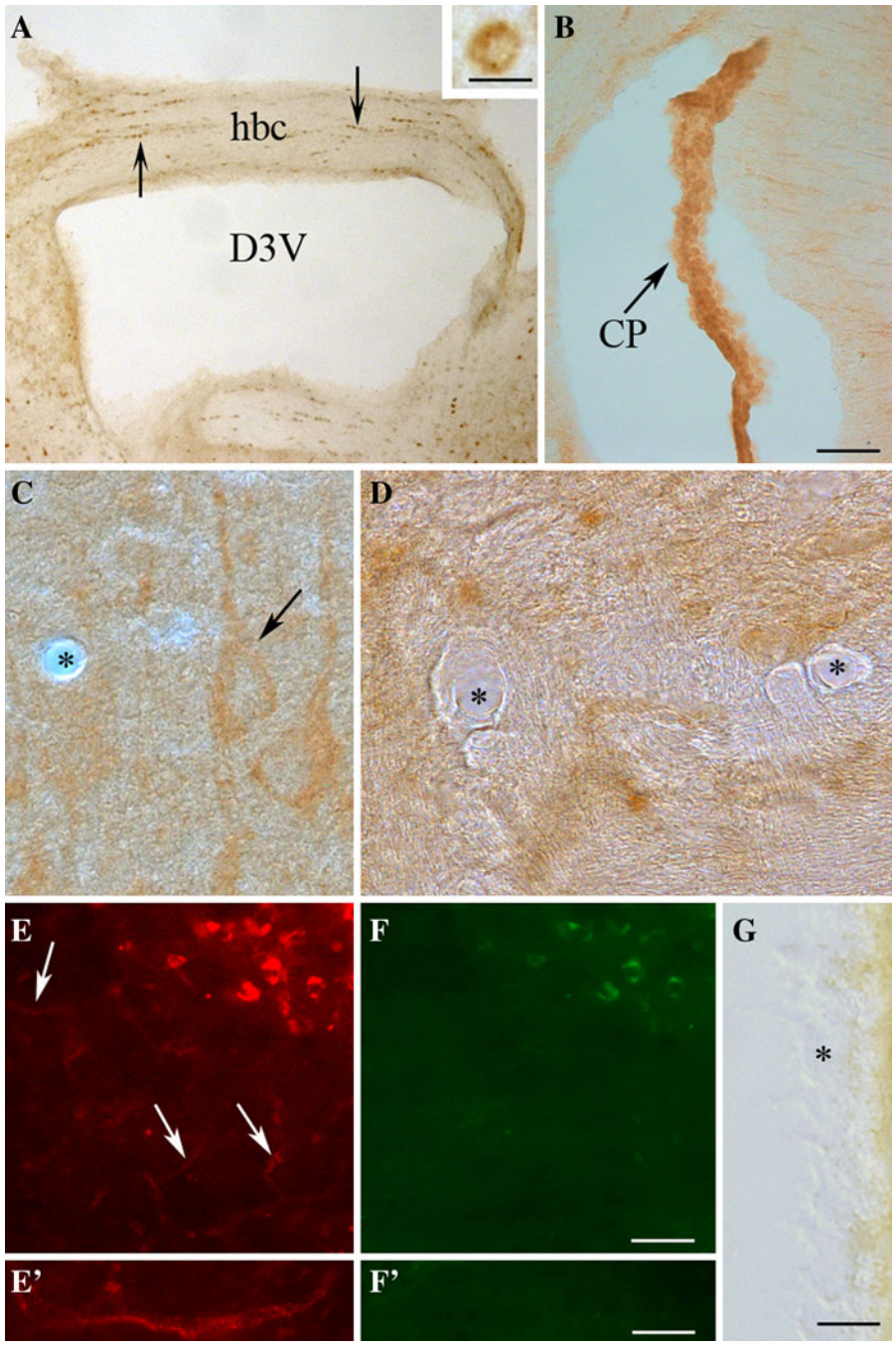

accessory olfactory bulb exhibited very strong Fpn-ir (Fig. 6; Table 1). These external plexiform layers contain apical dendrites of inhibitory granule cells that form large numbers of synapses with mitral cells and so-called tufted cells that regulate the spread of activity along the mitral—and tufted cell dendrites (Hamilton et al. 2005). Strong Fpn-ir was seen in the mitral layer of the accessory olfactory bulb. Moderate Fpn-ir was seen the internal plexiform layer of the olfactory bulb and the mitral layer of the olfactory bulb. A weak labeling was seen in the lateral olfactory tract, the dorsal lateral olfactory tract, and the glomerular layer

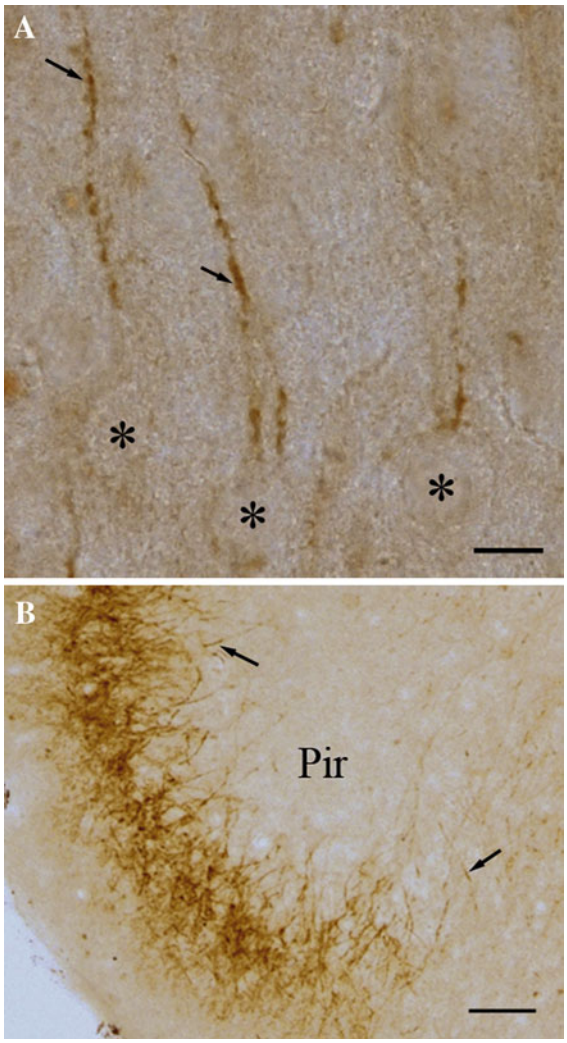

Fig. 4 Ferroportin-immunoreactivity (Fpn-ir) in the cerebral cortex. **a** Neurons of the primary motor cortex shown at high-power magnification. Immunolabeling is confined to proximal dendrites (*arrows*) with only weak labeling of the cytoplasma of the cell bodies. The neuronal nuclei (*asterisks*) are unlabeled. **b** The infero-lateral part of the cerebral cortex shown at medium-power magnification. Fpn-ir is present in fibers (*arrows*) of the piriform cortex (Pir). *Scale bars* **a** = 10 μm, **b** = 80 μm

(Fig. 6c). The latter contains fibers projecting from olfactory glomeruli to the mitral cells, and some of these fibers did exhibit strong Fpn-ir. Fpn-ir was absent from the granule cell layer of the olfactory bulb.

Diencephalon

In diencephalon, Fpn-ir was mainly detected in the thalamus (Figs. 7, 8). Labeling of many thalamic neurons was seen in cell bodies with a minimum of labeling of peripheral processes. Hence, a moderate Fpn-ir was detected in neuronal cell bodies in ventral posteromedial- and ventral posterolateral thalamic nuclei, and weakly in cell bodies of neurons of the reticular thalamic nucleus. An exception to these observations was made in neurons of the ventral medial thalamic nucleus that also exhibited Fpn-ir in peripheral processes (Fig. 7a). Fpn-ir was not observed in neurons of the subthalamic nucleus. In the hypothalamus, the Fpn-ir was weak with sparsely labeled neuronal cell bodies only in the dorsomedial hypothalamic nucleus, the paraventricular nuclei, and the supraoptic nucleus (not shown). In contrast, the fibers of the median eminence exhibited a marked Fpn-ir (Fig. 7b).

The most intense neuronal Fpn-ir in the entire brain was in the neurons of the medial habenular nucleus in the thalamus (Fig. 8a). Both cell bodies and axons projecting as the habenular interpeduncular tract to the interpeduncular nucleus were heavily labeled (Fig. 8b, c). In contrast, labeling of neurons in the lateral habenular nucleus was only seen in cell bodies.

Mesencephalon

Neuronal Fpn-ir was particularly well confined to the interpeduncular nucleus that harbored many densely labeled fibers (Fig. 8d). These fibers probably originate in the medial habenular nucleus as part of the habenulo-interpeduncular tract, because the axons of this tract exhibited consistent labeling (Fig. 8b). Fpn-ir was strong in cell bodies of the oculomotor nucleus (Fig. 9a), trochlear nucleus, and moderate in neurons of the superior colliculus, red nucleus, and substantia nigra pars compacta. Fpn-ir was weak in the neurons of the substantia nigra pars reticulata. The latter applied to neurons situated in the ventral tegmental area, and neurons of the mesencephalic trigeminal nucleus.

Pons

Neuronal Fpn-ir was mainly found in neuronal cell bodies. Strongly immunolabeled neurons were observed in motor neurons of the cranial nerve nuclei such as the motor trigeminal nucleus (Fig. 9b), nucleus abducens, and facial nucleus (Fig. 9c, d).

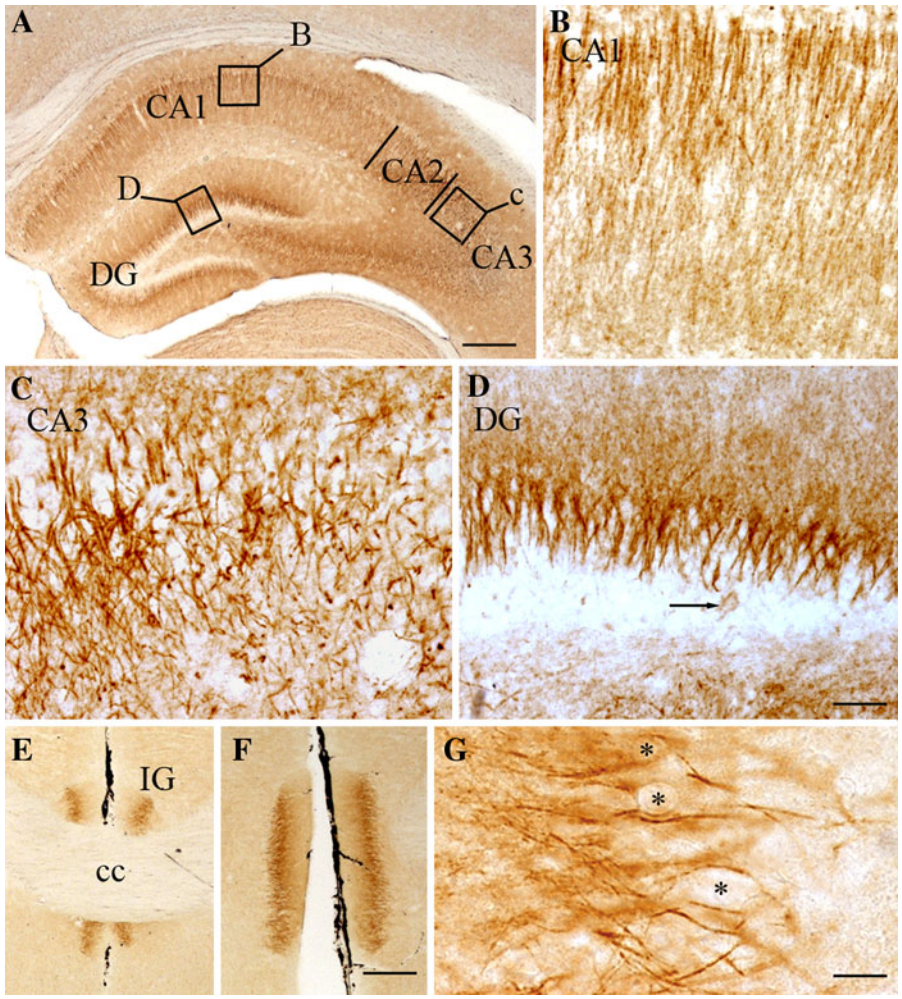

Fig. 5 Ferroportin-immunoreactivity (Fpn-ir) in the hippocampus. **a** The hippocampus proper shown at low-power magnification; note the prominent Fpn-ir in the hippocampal cortex. **b** Immunolabeling of the CA1 region. By far, the majority of Fpn-ir is confined to peripheral processes extending from the pyramidal cell layer. **c** The CA3 region. The Fpn-ir in neurons of the CA3 region is slightly lower than that seen in CA1. **d** Immunolabeling of the dentate gyrus (DG). The neurons of this region essentially reveal a distribution similar to that of the neurons of the CA1 region with a prominent labeling of the axons of the pyramidal cells. Labeling is also occasionally seen in interneurons of the white matter (*arrow*). **e**, **f** Fpn-ir in the indusium griseum (IG) shown at the level of the corpus callosum (cc) that separates this grey matter region in two (**e**) and at a slightly more distal level where the indusium griseum is found below the corpus callosum (**f**). **g** The indusium griseum shown at high magnification. Immunolabeling is confined to peripheral processes whereas the neuronal cell bodies are unlabeled (*asterisks*). *Scale bars* **a**, **e**, **f** = 120 μm; **b**, **c**, **d** = 40 μm; **g** = 15 μm

The neurons of motor trigeminal nucleus and facial nucleus exhibited more labeling in peripheral processes as compared to neurons of other cranial nerve nuclei like the oculomotor and trochlear nuclei (Fig. 9; Table 1). Fpn-ir was also detected in the small neurons of the pontine nucleus. A strong Fpn-ir was seen in neuronal cell bodies of the locus coeruleus (Fig. 10c).

Medulla oblongata

Prominent Fpn-ir was observed in neurons of vestibular and cochlear nuclei subsets. The labeling of these neurons was consistently confined to their cell bodies. Among cranial nerve nuclei, labeling was detected in cell bodies of the solitary tract nucleus, the ambiguus nucleus (Fig. 9e), and the hypoglossal nucleus. Slight

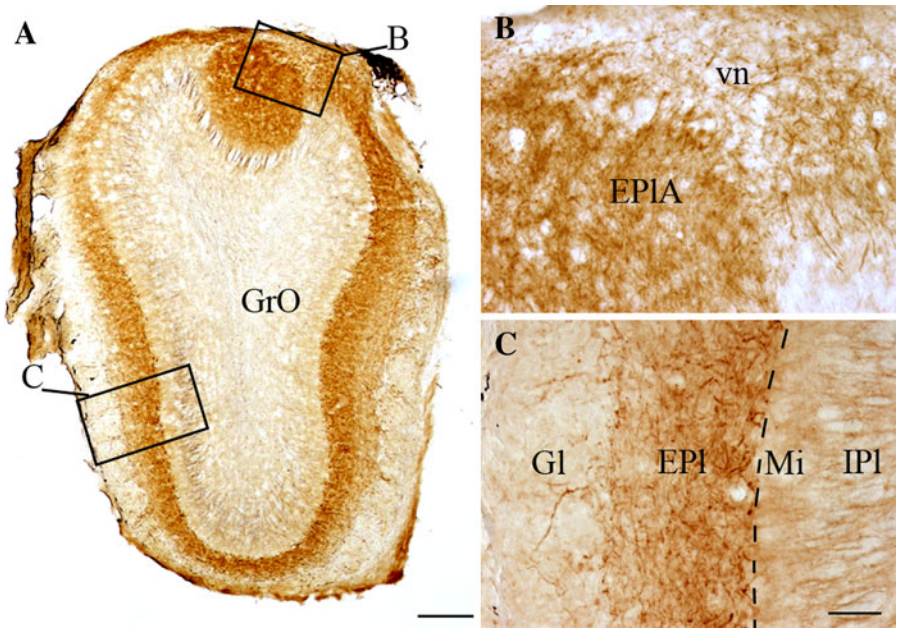

Fig. 6 Ferroportin-immunoreactivity (Fpn-ir) in the olfactory bulb and accessory olfactory bulb. **a** Transverse section shown at low-power magnification. Fpn-ir is mainly seen in projecting fibers. Neurons of the granule cell layer of the olfactory bulb (GrO) are unlabeled. The *marked area* are shown in larger magnification in **b** and **c**. **b** Area containing very strong Fpn-ir in projecting fibers of the external plexiform layer of the accessory olfactory bulb (EPlA). **c** Fpn-ir is very strong in the external plexiform layer of the olfactory bulb (EPl), moderate in the mitral cell layer (Mi) and internal plexiform layer (IPl), and weak in the glomerular layer (Gl). The Gl though contains very strongly immunolabeled Fpn-ir fibers transversing from the olfactory nerve to the EPl. *Scale bars* **a** = 120 μm; **b**, **c** = 40 μm

labeling was seen in neurons of the dorsal motor nucleus of the vagus, as well as in neurons of the sensory trigeminal nucleus and in neurons of the gracile and cuneate nuclei (not shown).

Reticular formation

Various neurons of the reticular formation presented an overall strong to very strong Fpn-ir in cell bodies and peripheral processes (Fig. 10). A very strong Fpn-ir was seen in neuronal processes of the dorsal raphe nucleus and rhabdoid nucleus (Fig. 10a). Neurons of these nuclei also had a weak expression of Fpn-ir in their cell bodies. In contrast, other neurons of the reticular formation like neurons of the pontine reticular nucleus exhibited a strong Fpn-ir in both neuronal cell bodies and proximal dendrites (Fig. 10b). The latter also applied to neurons of the ventral and laterodorsal tegmental nuclei (not shown). Moderate Fpn-ir was seen in peripheral processes of neurons contributing to the medial longitudinal fasciculus.

Cerebellum

In the cerebellar cortex, Fpn-ir was observed in Purkinje cells of the different lobules (Fig. 11a). The perikarya of the Purkinje cells and the proximal dendrites projecting into the molecular layer were very strongly labeled (Fig. 11b). The deep cerebellar nuclei, the medial, interposed and lateral (dentate) nuclei exhibited moderate Fpn-ir (Fig. 11c).

Discussion

Studies of the rat brain revealed that ferroportin is present in neurons of the cerebral cortex, hippocampus, and cerebellum, but not in regions like the striatum and thalamus (Burdo et al. 2001; Moos and Rosengren Nielsen 2006). In the human cerebellum, ferroportin was observed in neurons of the dentate nucleus (Koeppen et al. 2007). In studies of paraffin-embedded mouse brain, ferroportin expression was detected in discrete regions of the brain with

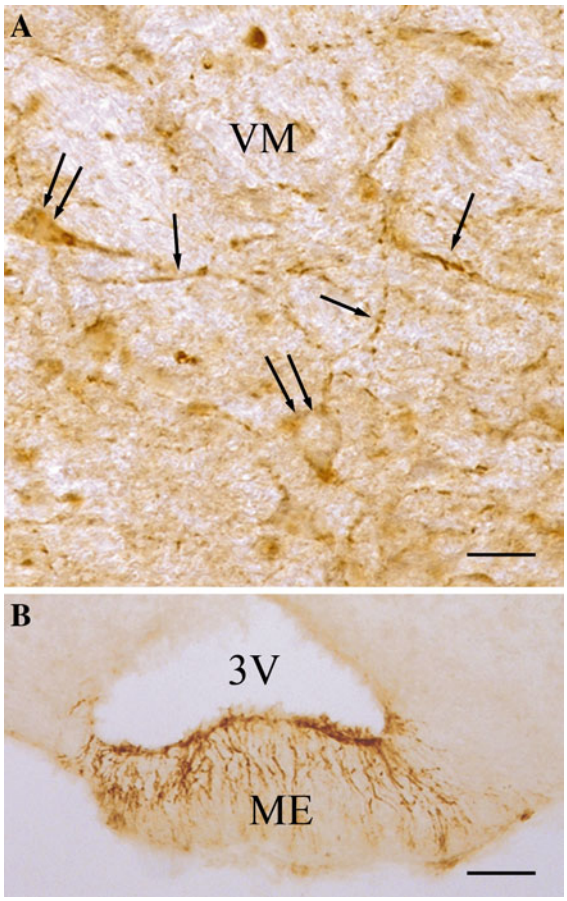

Fig. 7 Ferroportin-immunoreactivity (Fpn-ir) in the diencephalon. **a** In the ventral medial thalamic nucleus (VM), Fpn-ir is seen in both fibers (*arrows*) and cell bodies (*double arrows*). **b** Fpn-ir is scarce in the hypothalamus. This illustration depicts Fpn-ir in the median eminence (ME); one of the few areas of the hypothalamus to contain Fpn-ir. Note the dense fiber-like immunolabeling. 3V, third ventricle. *Scale bars* **a** = 20 μm, **b** = 80 μm

immunohistochemical techniques and in situ hybridization (Wu et al. 2004). We mapped the distribution of ferroportin by processing free-floating 40 μm thick sections immunohistochemically, which allows for a profound analysis of Fpn-ir in neuronal cell bodies and their projections in particular. Ferroportin was found in virtually all regions of the brain with the main exception being some regions of the basal forebrain and orbital cortex (Table 1). Among labeled cell bodies, ferroportin was predominantly expressed in Purkinje neurons of the cerebellar cortex, and in neurons of the brain stem in cranial nerve nuclei, neurons of the reticular formation, and the locus coeruleus. Reports have not been made on the presence of ferroportin in neurons of brain stem nuclei and reticular formation. The demonstration of the very strong Fpn-ir in neuronal projections of the olfactory pathways and reticular formation are also novel. These labeled fibers are all axons, but Fpn-ir was also observed in dendrites of, e.g., Purkinje cells and some reticular neurons.

The subcellular distribution of neuronal ferroportin

Wu et al. (2004) used biochemical analyses to verify the presence of ferroportin in neuronal membranes. Our data showing a robust Fpn-ir in membranes of dendrites and axons in several brain regions indicate that neurons may excrete ferrous iron from all over their surface. Moreover, the observation that the distribution of neuronal processes labeled with Fpn-ir is heterogeneous clearly suggests that the extent of iron excretion is much higher in some regions than others. Many regions of the limbic structures, like the hippocampal formation and olfactory pathways markedly express ferroportin suggesting a prominent iron export from peripheral processes. By contrast, neurons of other regions particularly those of the basal forebrain, basal ganglia, and some projecting fibers, e.g., those of the corpus callosum and pyramis only exhibited minor Fpn-ir. This weak immunoreactivity could be attributed to a reduced capability of the polyclonal anti-ferroportin antibody to label myelinated structures. However, when examining these structures in cross-sections a weak Fpn-ir was detected, which a priori should ease the capability of the antibody to target neuronal ferroportin, as the cross-sections invariably expose components of the neurons without wrapping of myelin. Fpn-ir was strong to very strong in cross-sections of peripheral processes of many neuronal structures, e.g., those of the olfactory bulb, hippocampus, and habenula. Therefore we find it less likely that the absence of Fpn-ir in neuronal cell bodies and peripheral processes of neurons of the basal forebrain, basal ganglia, and Fpn-ir in projecting fibers of the corpus callosum and pyramis is due to low sensitivity of the antibody to detect ferroportin. Neuronal cell bodies and processes of the latter structures are also much lower in transferrin receptors as compared to neurons elsewhere in the mouse brain (Moos 1996).

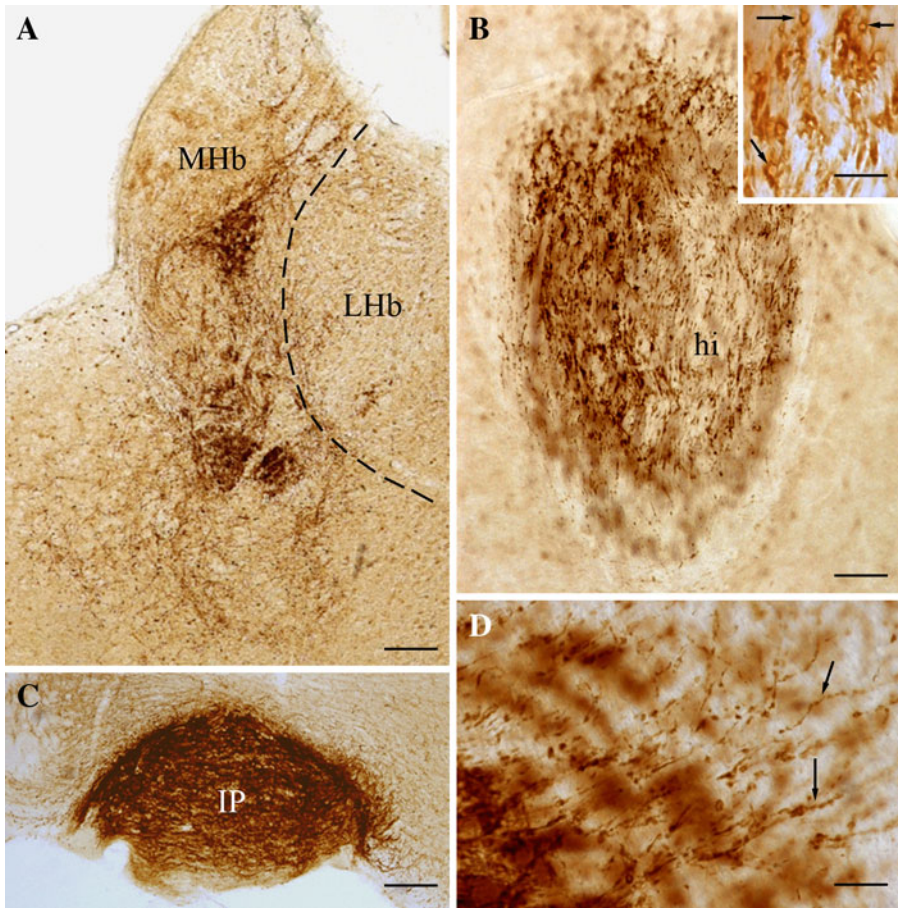

Fig. 8 Ferroportin-immunoreactivity (Fpn-ir) in neurons of the habenulo-interpeduncular tract. Neurons of the medial habenular nucleus (MHb) send their projections as the habenulo-interpeduncular (hi) tract to the interpeduncular nucleus (IP). **a** The habenular region containing Fpn-ir in neuronal cell bodies and fibers of the MHb. The LHb separated from the MHb with the dashed line does not contain Fpn-ir projecting fibers but has Fpn-ir confined to neuronal cell bodies. **b** The hi taken from a section at the level of the mesencephalon shown at medium-power magnification. Fpn-ir fibers are abundant. *Insert* Fpn-ir in axons shown at high-power magnification using Nomarski optics. Note that immunolabeling is confined to the cell membrane of the transversely sectioned axons (*arrows*). **c** The interpeduncular nucleus (IP) shown at medium-power magnification. **d** At high magnification, the Fpn-ir of the IP denotes a fiber-like distribution corresponding to immunolabeled axons of the habenulo-interpeduncular tract (*arrows*). *Scale bars* **a**, **c** = 40 μm; **b**, **d** = 80 μm; **b** *insert* = 5 μm

Neurons contain ferritin H + L mRNAs, ferritin protein (Benkovic and Connor 1993; Hansen et al. 1999), ferroportin mRNA (Wu et al. 2004) and ferroportin protein (Burdo et al. 2001; Wu et al. 2004; the present study) indicative of a co-expression of ferritin and ferroportin in neurons. The presence of ferroportin in axons of the hippocampal formation, however, is not accompanied by co-expression of ferritin (Benkovic and Connor 1993; Hansen et al. 1999) suggesting that iron is present in hippocampal axons in a dynamic pool. The presence of ferroportin in the axonal membrane may denote the prerequisite for a mechanism to excrete iron to keep its concentration inside the axon within a reasonable range. The absence of ferroportin in the striatum and pallidum could indicate that iron of the basal ganglia is present as ferric iron. Iron of the basal ganglia is histologically distributed to axons and oligodendrocytes and their wrappings, and its presence is accompanied by prominent expression of ferritin (Benkovic and Connor 1993). The oligodendrocytes could store iron in ferritin and not have a need to export iron and thus

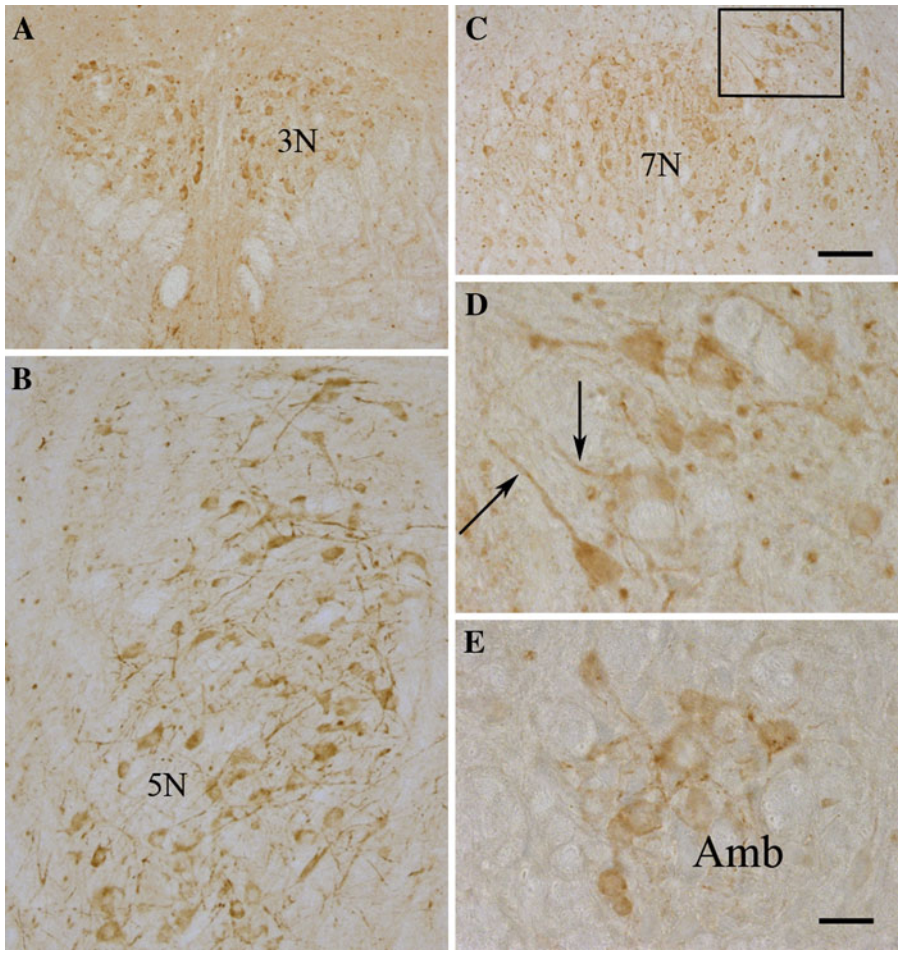

Fig. 9 Ferroportin-immunoreactivity (Fpn-ir) in motor neurons of cranial nerve nuclei. **a** Neurons of the oculomotor nucleus (3N). **b** Neurons of the motor trigeminal nucleus (5N). **c** The facial nucleus (7N). **d** Neurons of the facial nucleus marked in the framed area in **c** and shown at high-power magnification. **e** The ambiguus nucleus (Amb). The neurons of these cranial nerve nuclei exhibit Fpn-ir in both cell bodies and fibers. The labeling of the neuronal fibers is particularly evident in neurons of the motor trigeminal nucleus and facial nucleus. *Scale bars* **a**–**c** = 40 μm; **d**, **e** = 10 μm

downgrade ferroportin, while maintaining ferritin expression.

Unlike the heterogeneous co-distribution pattern with ferritin, neuronal ferroportin co-distributes with the transferrin receptor in that their distributional patterns in the brain seem to overlap (cf. Moos 1996). In contrast, their subcellular distribution patterns of ferroportin and transferrin receptors in neurons differ in that transferrin receptors are expressed on the surface of the cell body and dendrites, but not on the axon (cf. Moos 1996; West et al. 1997). Subsequent to the uptake of iron-containing transferrin at the soma and dendrites, iron, by means of anterograde axonal transport, most likely enters the axon in which ferroportin appropriately will participate in handling iron-levels.

The significance of ferroportin for neuronal iron export

Ferroportin's significance for neurons is thought to include a crucial function for exporting ferrous iron, whereby neurons regulate their intracellular iron level (Burdo et al. 2001; Moos et al. 2007; Wu et al. 2004). Regarding its significance, ferroportin is the sole protein that is known to export iron from cells, and its neuronal distribution as reported in the present and previous studies clearly indicates that ferroportin

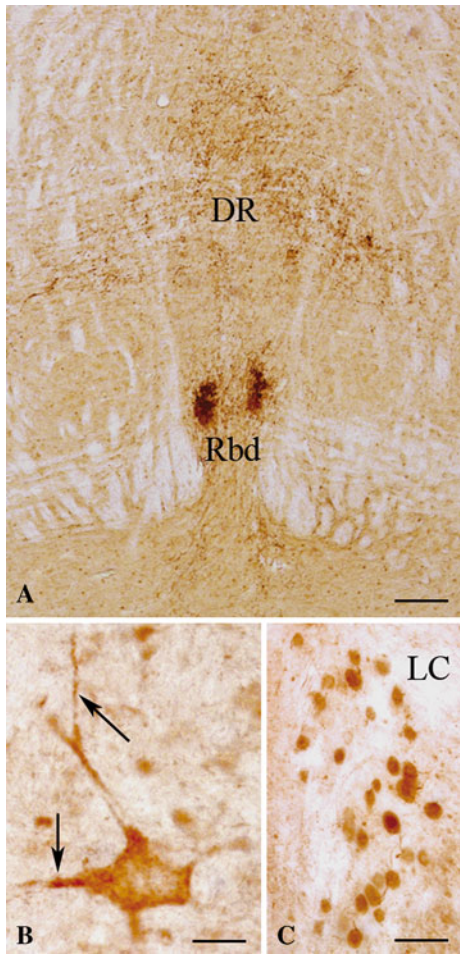

Fig. 10 Ferroportin-immunoreactivity (Fpn-ir) in neurons of the reticular formation and locus coeruleus. **a** Fpn-ir in neurons of the dorsal raphe nucleus (DR) and rhabdoid nucleus (Rbd) of the reticular formation. **b** Fpn-ir in a single reticular neuron of the pontine reticular nucleus. Note the strong labeling of the cell body and proximal dendrites (*arrows*). **c** Fpn-ir neuronal cell bodies of the locus coeruleus (LC) are also strongly labeled. *Scale bars* **a** = 80 μm, **b** = 10 μm, **c** = 40 μm

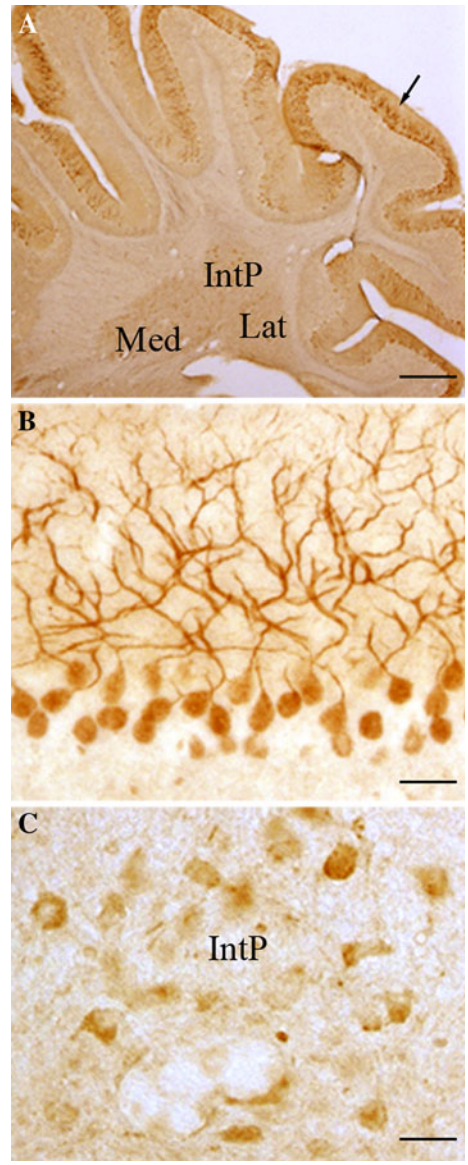

Fig. 11 Ferroportin-immunoreactivity (Fpn-ir) in the cerebellum. **a** The cerebellum shown at low-power magnification. Fpn-ir is mainly seen in the cerebellar cortex (*arrow*) and neurons of the deep cerebellar nuclei (Med, medial nucleus; IntP, interposed nucleus posterior part; Lat, lateral nucleus). **b** Very strongly labeled Fpn-ir in cell bodies and dendrites of Purkinje cells of the cerebellar cortex. **c** Fpn-ir in neurons of the IntP shown at high-power magnification. Moderate immunolabeling is seen in cell bodies. *Scale bars* **a** = 120 μm; **b**, **c** = 20 μm

must play an important role in the excretion of iron from the neuron (Burdo et al. 2001; Moos and Rosengren Nielsen 2006; Wu et al. 2004). The export of iron may well involve the presence of a neuronal ferrous oxidase that prevents ferrous iron from entering the brain's extracellular space where it could otherwise induce oxidative stress on adjacent cell membranes (cf. Moos et al. 2007).

There is little available data on ferroportin in brains with experimentally altered iron concentrations. The mRNA of the iron exporter ferroportin contains an iron-responsive element in its 5′ untranslated region (UTR) and has an expression pattern similar to that of ferritin. Belgrade rats mutated in the divalent metal transporter 1 (DMT 1) gene suffer

from an insufficient iron uptake by the brain (Farcich and Morgan 1992). The brains of these rats exhibit unaltered levels of ferroportin (Burdo et al. 2001). Wu et al. (2004) studied mice with a mutated iron-regulatory protein (IRP) 2, which leads to neurodegeneration and regional increases in brain iron, but found no changes in the expression of ferroportin. The absence of any such changes could be explained by the fact that the concentration of iron does not change significantly enough in these mutants. The amount of ferroportin protein in neurons and oligodendrocytes would hypothetically decrease during episodes of iron deficiency and increase with ample iron. Ferroportin expression in the brain should be addressed in experimental models with dietary iron-deficiency and signs of aging, because under these conditions the concentration of brain iron changes significantly (Focht et al. 1997; Moos et al. 1998).

The hormone hepcidin exerts post-translational regulation of the ferroportin protein. Macrophages, monocytes, and enterocytes all have their content of ferroportin down-regulated under the influence of hepcidin which internalizes together with ferroportin. This leads to ferroportin degradation and redistribution from the cellular membrane to the cytoplasm, leaving the cell less prone to excrete iron (Nemeth et al. 2004). Pathological brain conditions that involve compromised blood–brain barrier integrity are accompanied by extravasation of blood plasma and migration of inflammatory cells into the brain; hepcidin undoubtedly also enters the brain with the potential to reduce the expression of ferroportin. Hepcidin is widely expressed in the normal murine brain and injection of hepcidin into the brain will cause a reduction of ferroportin (Wang et al. 2009). This observation supports the idea that hepcidin entering the brain in pathological conditions will affect ferroportin.

Ferroportin in non-neuronal cells in the brain

The detection of iron-related proteins in non-neuronal cells in vivo has generally proved to be a major challenge. The exception is transferrin and ferritin that evidently are expressed and shown at both mRNA and protein levels in oligodendrocytes and microglia (Benkovic and Connor 1993). Limitations in the detection levels of proteins probably might be responsible for the controversy on whether or not iron-related proteins are expressed in glial cells. Hence, it remains a paradox that in vivo transferrin receptors are undetectable in oligodendrocytes and microglia, and DMT 1 and ceruloplasmin are inconsistently detected in astrocytes (Huang et al. 2006; Klomp et al. 1996; Moos et al. 2006), as these proteins are detected in vitro (Jeong and David 2003; Patel and David 1997). Transferrin receptors are indeed expressed by cultured oligodendrocytes (Todorich et al. 2008), as are DMT 1 and ceruloplasmin by cultured astrocytes (Jeong and David 2003; Lis et al. 2004; Patel and David 1997). The capability to export ferrous iron from cultured astrocytes expressing ferroportin was recently shown to depend on a stabile expression of ceruloplasmin (De Domenico et al. 2007).

In the present study, ferroportin was consistently observed in oligodendrocytes. Similar observations were reported in studies of the rat brain (Burdo et al. 2001; Moos and Rosengren Nielsen 2006), but contradict the observations made by Wu et al. (2004) and Rouault et al. (2009). The present study used an antibody that specifically detects mouse ferroportin as observed in many non-neuronal tissues (Abboud and Haile 2000). The detection of its specific binding to ferroportin in the mouse brain was additionally enhanced with biotinylated tyramide and revealed a profound immunoreaction with a minimum of non-specific background labeling. Probably this indicates that if astrocytes or microglia contain the ferroportin protein, their labeling is extremely scarce. The presence of ferroportin in the cell bodies suggests that oligodendrocytes refrain from excreting ferrous iron in their peripheral processes. The iron-metabolism of oligodendrocytes is far from resolved, but the present data might indicate that iron transported to the periphery is not capable of being secreted unless transported back to the cell body by a mechanism equivalent to retrograde axonal transport in neurons (Moos et al. 2007). The content of ferritin in oligodendrocytes rises with increasing age (Focht et al. 1997), which could indicate that their capacity for cellular transport and excretion of iron diminishes. This might lead to an increased risk of free radical-mediated oxidative stress with age due to a reduction in the oligodendrocytes' ability to handle iron.

The detection of a weak but consistent signal of ferroportin mRNA in the cultured bEnd3 cells might

indicate that the Fpn protein is also expressed in endothelial cells in vivo, although at very low levels, as immunohistochemistry failed to detect Fpn in brain capillary endothelial cells in vivo both in the mouse (the present study) and rat (Moos and Rosengren Nielsen 2006). The failure to detect Fpn protein in brain capillary endothelial cells suggests that ferroportin is devoid of major significance for iron export from endothelial cells in the brain and supports the idea that iron gets transported through the blood–brain barrier to enter the brain as ferric iron (cf. Moos et al. 2007).

The discrepancy in the detection of ferroportin in choroid plexus epithelial cells as observed in the studies of Wu et al. (2004), Burdo et al. (2001), Moos and Rosengren Nielsen (2006), Rouault et al. (2009) and the present study probably rely on differences in detection levels. Ferroportin protein was detected in choroid plexus of the human brain together with hepcidin in the cerebrospinal fluid (Clardy et al. 2006), and ferroportin mRNA and protein was detected in the choroid plexus of the mouse brain (Wu et al. 2004; Rouault et al. 2009). The choroid plexus express transferrin receptors (Moos 1996), and receptor-mediated endocytosis of transferrin by the choroid plexus is likely followed by detachment of iron from transferrin within the choroid plexus epithelial cells beside from being transported through the choroid plexus by transcytosis (Moos and Morgan 1998). The ferroportin expression probably reflects the capability of the choroid plexus to export ferrous iron into the cerebrospinal fluid of the ventricular system.

Acknowledgments We would like to thank Susan Peters at University of Copenhagen, Denmark and Merete Fredsgaard, Aalborg University, Denmark for excellent technical assistance. Murine brain endothelioma cells, bEnd3, were kindly obtained from Dr. Sara Gosk, University of Bonn, Germany. This work was supported by grants from the Lundbeck Fund, the Danish Parkinson's Disease Fund, the Carlsberg Foundation, the Spar Nord Fund, and the Obelske Familiefond.

References

Abboud S, Haile DJ (2000) A novel mammalian iron-regulated protein involved in intracellular iron metabolism. J Biol Chem 275:19906–19912

Adamek GD, Shipley MT, Sanders MS (1984) The indusium griseum in the mouse: architecture, Timm's histochemistry and some afferent connections. Brain Res Bull 12:657–668

Altamura S, Muckenthaler MU (2009) Iron toxicity in diseases of aging: Alzheimer's disease, Parkinson's disease and atherosclerosis. J Alzheimers Dis 16:879–895

Balin BJ, Broadwell RD, Salcman M, el-Kalliny M (1986) Avenues for entry of peripherally administered protein to the central nervous system in mouse, rat, and squirrel monkey. J Comp Neurol 251:260–280

Benkovic SA, Connor JR (1993) Ferritin, transferrin, and iron in selected regions of the adult and aged rat brain. J Comp Neurol 338:97–113

Burdo JR, Menzies SL, Simpson IA, Garrick LM, Garrick MD, Dolan KG, Haile DJ, Beard JL, Connor JR (2001) Distribution of divalent metal transporter 1 and metal transport protein 1 in the normal and Belgrade rat. J Neurosci Res 66:1198–1207

Chua AC, Graham RM, Trinder D, Olynyk JK (2007) The regulation of cellular iron metabolism. Crit Rev Clin Lab Sci 44:413–459

Clardy SL, Wang X, Boyer PJ, Earley CJ, Allen RP, Connor JR (2006) Is ferroportin-hepcidin signaling altered in restless legs syndrome? J Neurol Sci 247:173–179

Crichton R (2009) Iron metabolism: from molecular mechanisms to clinical consequences. Wiley, Chichester

De Domenico I, Ward DM, di Patti MC, Jeong SY, David S, Musci G, Kaplan J (2007) Ferroxidase activity is required for the stability of cell surface ferroportin in cells expressing GPI-ceruloplasmin. EMBO J 26:2823–2831

Donovan A, Brownlie A, Zhou Y, Shepard J, Pratt SJ, Moynihan J, Paw BH, Drejer A, Barut B, Zapata A, Law TC, Brugnara C, Lux SE, Pinkus GS, Pinkus JL, Kingsley PD, Palis J, Fleming MD, Andrews NC, Zon LI (2000) Positional cloning of zebrafish ferroportin 1 identifies a conserved vertebrate iron exporter. Nature 403:776–781

Donovan A, Lima CA, Pinkus JL, Pinkus GS, Zon LI, Robine S, Andrews NC (2005) The iron exporter ferroportin/Slc40a1 is essential for iron homeostasis. Cell Metab 1:191–200

Farcich EA, Morgan EH (1992) Diminished iron acquisition by cells and tissues of Belgrade laboratory rats. Am J Physiol 262:R220–R224

Focht SJ, Snyder BS, Beard JL, Van Gelder W, Williams LR, Connor JR (1997) Regional distribution of iron, transferrin, ferritin, and oxidatively-modified proteins in young and aged Fischer 344 rat brains. Neuroscience 79:255–261

Franklin KBJ, Paxinos G (2008) The mouse brain in stereotaxic coordinates, 3rd edn. Elsevier, Amsterdam

Gosk S, Moos T, Gottstein C, Bendas G (2008) VCAM-1 directed immunoliposomes selectively target tumor vasculature in vivo. Biochim Biophys Acta 1778:854–863

Hamilton KA, Heinbockel T, Ennis M, Szabó G, Erdélyi F, Hayar A (2005) Properties of external plexiform layer interneurons in mouse olfactory bulb slices. Neuroscience 133:819–829

Hansen TM, Nielsen H, Bernth N, Moos T (1999) Expression of ferritin protein and subunit mRNAs in normal and iron deficient rat brain. Brain Res Mol Brain Res 65:18–197

Huang E, Ong WY, Go ML, Connor JR (2006) Upregulation of iron regulatory proteins and divalent metal transporter-1 isoforms in the rat hippocampus after kainate induced neuronal injury. Exp Brain Res 170:376–386

Jeong SY, David S (2003) Glycosylphosphatidylinositol-anchored ceruloplasmin is required for iron efflux from cells in the central nervous system. J Biol Chem 278:27144–27148

Jeong SY, Rathore KI, Schulz K, Ponka P, Arosio P, David S (2009) Dysregulation of iron homeostasis in the CNS contributes to disease progression in a mouse model of amyotrophic lateral sclerosis. J Neurosci 29:610–619

Klomp LW, Farhangrazi ZS, Dugan LL, Gitlin JD (1996) Ceruloplasmin gene expression in the murine central nervous system. J Clin Invest 98:207–215

Koeppen AH, Michael SC, Knutson MD, Haile DJ, Qian J, Levi S, Santambrogio P, Garrick MD, Lamarche JB (2007) The dentate nucleus in Friedreich's ataxia: the role of iron-responsive proteins. Acta Neuropathol 114:163–173

Lis A, Barone TA, Paradkar PN, Plunkett RJ, Roth JA (2004) Expression and localization of different forms of DMT1 in normal and tumor astroglial cells. Brain Res Mol Brain Res 122:62–70

McKie AT, Marciani P, Rolfs A, Brennan K, Wehr K, Barrow D, Miret S, Bomford A, Peters TJ, Farzaneh F, Hediger MA, Hentze MW, Simpson RJ (2000) A novel duodenal iron-regulated transporter, IREG1, implicated in the basolateral transfer of iron to the circulation. Mol Cell 5:299–309

Moos T (1996) Immunohistochemical localization of intraneuronal transferrin receptor immunoreactivity in the adult mouse central nervous system. J Comp Neurol 25:675–692

Moos T, Morgan EH (1998) Kinetics and distribution of [^{59}Fe-^{125}I]transferrin injected into the ventricular system of the rat. Brain Res 790:115–128

Moos T, Rosengren Nielsen T (2006) Ferroportin in the postnatal rat brain: implications for axonal transport and neuronal export of iron. Semin Pediatr Neurol 13:149–157

Moos T, Oates PS, Morgan EH (1998) Expression of the neuronal transferrin receptor is age dependent and susceptible to iron deficiency. J Comp Neurol 398:420–430

Moos T, Skjoerringe T, Gosk S, Morgan EH (2006) Brain capillary endothelial cells mediate iron transport into the brain by segregating iron from transferrin without the involvement of divalent metal transporter 1. J Neurochem 98:1946–1958

Moos T, Rosengren Nielsen T, Skjørringe T, Morgan EH (2007) Iron trafficking inside the brain. J Neurochem 103:1730–1740

Nemeth E, Tuttle MS, Powelson J, Vaughn MB, Donovan A, Ward DM, Ganz T, Kaplan J (2004) Hepcidin regulates cellular iron efflux by binding to ferroportin and inducing its internalization. Science 306:2090–2093

Patel BN, David S (1997) A novel glycosylphosphatidylinositol-anchored form of ceruloplasmin is expressed by mammalian astrocytes. J Biol Chem 272:20185–20190

Rouault TA, Cooperman S (2006) Brain iron metabolism. Semin Pediatr Neurol 13:142–148

Rouault TA, Zhang DL, Jeong SY (2009) Brain iron homeostasis, the choroid plexus, and localization of iron transport proteins. Metab Brain Dis 24:673–684

Todorich B, Zhang X, Slagle-Webb B, Seaman WE, Connor JR (2008) Tim-2 is the receptor for H-ferritin on oligodendrocytes. J Neurochem 107:1495–1505

Todorich B, Pasquini JM, Garcia CI, Paez PM, Connor JR (2009) Oligodendrocytes and myelination: the role of iron. Glia 57:467–478

Wang SM, Fu LJ, Duan XL, Crooks DR, Yu P, Qian ZM, Di XJ, Li J, Rouault TA, Chang YZ (2009) Role of hepcidin in murine brain iron metabolism. Cell Mol Life Sci 67:123–133

West AE, Neve RL, Buckley KM (1997) Identification of a somatodendritic targeting signal in the cytoplasmic domain of the transferrin receptor. J Neurosci 17:6038–6047

Wu LJ, Leenders AG, Cooperman S, Meyron-Holtz E, Smith S, Land W, Tsai RY, Berger UV, Sheng ZH, Rouault TA (2004) Expression of the iron transporter ferroportin in synaptic vesicles and the blood-brain barrier. Brain Res 1001:108–117

Zecca L, Youdim MB, Riederer P, Connor JR, Crichton RR (2004) Iron, brain ageing and neurodegenerative disorders. Nat Rev Neurosci 5:863–873

Zhu X, Su B, Wang X, Smith MA, Perry G (2007) Causes of oxidative stress in Alzheimer disease. Cell Mol Life Sci 64:2202–2210

Zohn IE, De Domenico I, Pollock A, Ward DM, Goodman JF, Liang X, Sanchez AJ, Niswander L, Kaplan J (2007) The flatiron mutation in mouse ferroportin acts as a dominant negative to cause ferroportin disease. Blood 109:4174–4180